Modeling of pyrolytic laser direct writing: Noncoherent structures and instabilities

N. Arnold,[a] P. B. Kargl, and D. Bäuerle
Angewandte Physik, Johannes Kepler Universität, Linz, A-4040, Linz, Austria

(Received 31 January 1997; accepted for publication 1 May 1997)

Three-dimensional simulations of pyrolytic laser direct writing from gas-phase precursors are presented. They are based on a fast method for the calculation of temperature distributions induced by an energy beam in deposits of arbitrary shape. Analytical approximations, fast Fourier transform, and the multigrid technique are combined in the algorithm. Temperature dependences of the absorptivities and heat conductivities of the deposit and the substrate have been taken into account. Self-consistent modeling of the growth process allows one to explain oscillations in the height and width of lines caused by the feedback between the shape of the deposit, the temperature distribution, and the growth rate. For the deposition of W from an admixture of WCl_6+H_2 and a-SiO_2 substrates, the oscillations originate from a sharp increase in the absorptivity of the deposit with temperature. With the deposition of Si from SiH_4, or C from CH_4, C_2H_2, and C_2H_4, onto a-SiO_2, the oscillations are related to the large ratio of height/width of the deposit and the increase in temperature on its upper surface. This increase also explains the transition from line-type to fiber-type growth. The hysteresis of this transition with respect to laser power and scanning velocity is explained as well. The same algorithm can be used in the modeling of pyrolytic etching and e-beam microprocessing when the feedback between the temperature distributions and changes in the processing geometry is important. © *1997 American Institute of Physics.* [S0021-8979(97)07415-X]

I. INTRODUCTION

Pyrolytic laser-assisted chemical vapor deposition (LCVD) has attracted attention in the last decade as a versatile tool for micromechanics and microdevice fabrication, wiring, customization and repair of interconnects, etc.[1,2] Deposition of many materials onto various substrates has been reported.[1,2] Different types of so-called noncoherent structures (not related to light interference phenomena) were observed.[3–8] The understanding of these structures, as well as the self-consistent description of the pyrolytic LCVD itself require a knowledge of the laser-induced temperature distribution and the modeling of the growth process. *In situ* temperature measurements are difficult to perform,[9] mainly due to the small size of the reaction zone. Thus, model calculations become quite useful. Here, however, the following problem arises. The presence of the deposit may change the temperature distribution drastically, especially if the deposit is ''thick'' (with a large height/width ratio) and its thermal conductivity is much higher than that of the substrate. This is often the case for the deposition of metals or semiconductors on insulators. Therefore, any realistic modeling of pyrolytic LCVD should include the (time-dependent) influence of the deposited material on the temperature distribution.

Laser-induced temperature distributions for regular geometries can, in many cases, be calculated analytically.[1,10,11] For a fixed geometry of the deposit, a number of numerical studies have been performed.[12,13] Self-consistent treatments of laser direct writing, which combine temperature and growth rate calculations, have been performed numerically[14] and on the basis of a simplified one-dimensional (1D) model.[15,16] In Ref. 17, we proposed a fast algorithm for the calculation of temperature distributions within arbitrarily shaped deposits. Temperature distributions in deposits such as dots and lines were calculated, and the growth process was simulated. In the present article, we apply this algorithm to realistic deposits. Several types of noncoherent oscillations and instabilities observed in laser direct writing are explained.

II. NUMERICAL PROCEDURE

Let us first enumerate the main ideas of the algorithm[17] for fast calculations of temperature distributions within deposits growing on semi-infinite substrates.

The temperature distribution at each moment is calculated from the *stationary* heat conduction equation. This is practically always justified in *micro*processing. The temperature dependence of the heat conductivities is eliminated by introducing linearized temperatures θ_S (for the substrate) and θ_D (for the deposit) via the Kirchhoff transform, which eliminates temperature-dependent heat conductivities $K(T)$ from the *stationary* heat conduction equations.[1,17] Then, the Poisson equation for the semi-infinite substrate and the deposit must be solved. The Green's function technique allows one to relate analytically θ_S at the surface of the *semi-infinite* substrate and its derivative along the normal to this surface. The heat equation for the *nonplanar deposit* is integrated in the direction perpendicular to the substrate surface with two different weight functions. This results in two equations for the moments of the temperature distribution θ_D. In a first approximation, this procedure describes a thermally thin deposit. A more refined approach takes into account temperature differences within the deposit and allows one to write a nonlinear integrodifferential equation for the temperatures at the substrate–deposit and deposit–ambient interfaces only,

[a]Electronic mail: nikita.arnold@jk.uni_linz.ac.at

 0021-8979/97/82(3)/1018/8/$10.00

i.e., equations for two-dimensional (2D) functions, instead of three-dimensional functions as in the initial problem. Besides, the integrals in these equations have the form of 2D convolutions; this permits the use of fast Fourier transform (FFT) techniques for numerical calculations. This enables one to develop a fast iterative procedure for the calculation of temperatures in the deposits with arbitrary shapes.

When the linearized temperature at the surface of the deposit $\theta_D^h(x,y)$ (x, y are the coordinates in the plane of the substrate) is known, it can be recalculated into the temperature $T^h(x,y)$ via the inverse Kirchhoff transform.[1,17]

Our goal is to apply this algorithm to the description of laser direct writing. For this reason, we write the equation of growth in the coordinate system fixed with the laser beam (positioned at $x=0$, $y=0$). The beam moves with respect to the substrate in the positive x direction with the scanning velocity v_s

$$\frac{\partial h}{\partial t} = W(T^h)[1+(\nabla h)^2]^{1/2} + v_s \frac{\partial h}{\partial x}. \tag{2.1}$$

Here, $h(x,y,t)$ is the height of the deposit, ∇h is the 2D gradient of the height in the $x-y$ plane, and W is the growth rate at the particular point, which is assumed to depend on temperature only. The term under the square root accounts for the fact that growth takes place along the normal to the deposit at each point.[18,19] For ''flat'' deposits with $\nabla h \ll 1$, this term can be neglected.

Equation (2.1) is solved numerically by the finite differences on a mesh, which is taken to be uniform, in order to use the FFT for the temperature calculations. The equation is split up into two parts, the growth part and the advective part (second term on the right side). The advection was performed by shifting the height array one spatial mesh step dx to the negative x direction after a constant time interval $\tau = dx/v_s$. This is a standard upwind scheme, which allows avoiding any distortion of Fourier harmonics during advection.[20]

The growth part of the problem can be treated numerically in different ways. In the simplest approach, the height is calculated at the new time step by the explicit scheme. Here, the temperature $T^h(h)$ is calculated for the height profile at the previous time step by the algorithm.[17] ∇h is calculated by symmetric differences $\partial h/\partial x = (h_{i+1} - h_{i-1})/2dx$, etc.

Another approach is similar to the two-step Lax–Wendroff procedure.[20] Here, each time step dt for the growth process is subdivided into two half steps. For the first half step, ∇h is calculated from the four nearest points comprising a rectangle in the $x-y$ grid. After that, the half-step height in the middle of a rectangle is determined by the explicit scheme. Here, the temperature that is used in the rate function in the center of the mesh rectangle is taken as an average from the temperature in its corners. Then, the half-step temperature is calculated for the half-step height and finally, the full-step height is calculated by using the half-step temperature in the rate function, and half-step height for the calculation of ∇h (also by the four points of the rectangle). Because this scheme has second-order accuracy in time, it permits bigger time steps. Other variations of this two-step procedure were tried as well. Variable time steps were usually employed with the limitations for the maximal possible relative and/or absolute increase in height per step. The reliability of the computational procedure was controlled by changing discretization, time steps, and accuracy in a wide range.

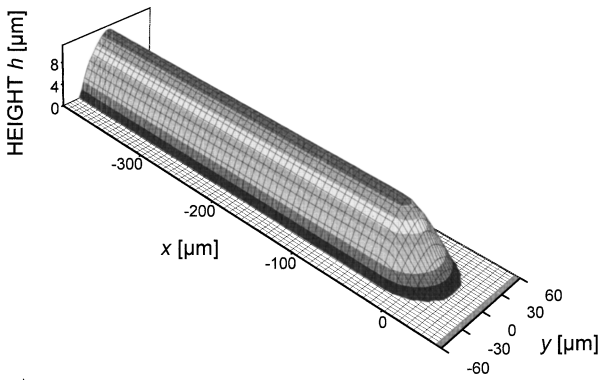

FIG. 1. Simulated height profile of a W line deposited from $WCl_6/H_2/O_2$ onto a-SiO_2. Surface absorption with *constant* absorptivity $A=0.6$, $w_0=7.5$ μm, $P=0.65$ W, and $v_s=15$ μm/s have been assumed. For the thermophysical parameters and growth rate dependence on temperature see Table I.

The most time-consuming part of the algorithm (temperature calculations) has iterative character.[17] This significantly decreases the computational time, because the geometry of the deposit changes only slightly during one time step.

III. OSCILLATIONS DUE TO CHANGES IN ABSORPTIVITY WITH TEMPERATURE

Oscillations in the width and height of stripes deposited on glass substrates by pyrolytic laser direct writing of W from WCl_6H_2 were reported for the first time in Ref. 21. This effect was studied in further detail in Ref. 6. It was found that during deposition, the absorptivity of the deposited tungsten changes almost twice, most probably due to the presence of a very small amount of oxygen in the reaction chamber.

A semiquantitative explanation of this effect was given in Ref. 22. The physical mechanism for the oscillations is the following: with constant absorptivity, lines are uniform. However, if the absorptivity increases with temperature in a certain temperature interval, the temperature, and thus, the growth rate spontaneously increase. This leads to an increase in the cross section of the deposited line and a subsequent temperature drop due to the increase in the heat transport along the line. Then the process repeats. For the existence of the oscillations, it is necessary that the increase in absorptivity with temperature is sharp enough, i.e., the energy input into the system increases faster than the energy losses.

Subsequently, we apply the developed numerical algorithm to the quantitative modeling of the oscillations observed.

If absorptivity A does not change with temperature, a uniform line is produced (Fig. 1). The parameters employed

TABLE I. Thermophysical and kinetic parameters of the materials considered in the calculations. Thermal conductivities were approximated by power functions $K(T)=K(T_0)(T/T_0)^n$.

Parameter: Units: Material	T_0 (K)	n	$K(T_0)$ (W/cm K)	Formula for $W(T)$	W_0 (μm/s)	T_a (K)	T_{th} (K)	δT_{th} (K)	α
a-SiO_2	300	0.57	0.0123						
	443	0.57	0.0154						
W from $WCl_6/H_2/O_2$	443	−0.29	0.78	(3.1)	16.05	2525	1200	15	
Si from SiH_4	300	−1.22	1.54	(4.1), (5.1)	2×10^8	22000			8×10^5

in the numerical calculations are listed in the Table I and in the figure captions. The following growth rate was used

$$W(T)=W_0\ \exp\left(-\frac{T_a}{T}\right)\left[\exp\left(\frac{T_{\mathrm{th}}-T}{\delta T_{\mathrm{th}}}\right)+1\right]^{-1}. \qquad (3.1)$$

Here, T_{th} characterizes the threshold temperature at which deposition starts,[23] δT_{th} defines the sharpness of this threshold, T_a is the Arrhenius activation temperature, and W_0 the corresponding preexponential factor.

The main features of deposition with constant absorptivity are the following: The *temperature* near the position of the laser beam *increases with the scanning velocity*, due to the decrease in the cross section of the stripe, which is a good heat conductor. The height and width of the deposited lines are almost proportional to the laser power. For this reason, the deposition *temperature* of the stripes, which are wider than the laser beam spot size w_0, *depends only slightly on laser power*. For the deposition of W from WCl_6/H_2, there exists a sharp threshold temperature. As a result, the width of the stripes depends on v_s in a nonmonotonous way, first it increases, and then it decreases. A detailed explanation of this behavior can be found in Refs. 15 and 16.

If the absorptivity $A(T)$ sharply increases near a certain temperature T_{Ab} (subscript ''Ab'' stands for absorptivity), and if the laser-induced temperature near the beam center is close to T_{Ab}, oscillations may arise. Henceforth, we use a steplike function

$$A(T)=A_0+A_1\left[\exp\left(\frac{T_{\mathrm{Ab}}-T}{\delta T_{\mathrm{Ab}}}\right)+1\right]^{-1}, \qquad (3.2)$$

where the absorptivity increases within the temperature interval δT_{Ab} near T_{Ab}, A_0 is the absorptivity at low temperatures, and A_1 the absolute change in absorptivity. The exact behavior of $A(T)$ outside of the region around T_{Ab} is unimportant, and Eq. (3.2) can be thereby employed in many cases. The increase in absorptivity can have different physical origins. It may be related to the microstructure of the deposit, to its chemical composition, the formation of a thin oxide layer, etc.[22]

The calculated line shape and temperature profile are shown in Figs. 2(a) and 2(b). The line profile agrees quite well with that experimentally observed (Fig. 3), (for more details see also Refs. 6 and 1). The temporal evolution of the calculated deposition process can be described as follows. When the cross section of the stripe becomes large, the temperature drops, and the absorptivity decreases to the lowest value A_0. Then, the deposition practically ceases until the laser beam reaches the edge of the deposit. Subsequently, both the temperature and the absorptivity increase, and a new deposition ''burst'' occurs. Here, the deposition proceeds ahead of the laser beam. A similar behavior was observed in Ref. 6. The highest temperature is achieved in this phase, which explains the experimental findings that the line*width* has minimum values slightly *after* the regions with the maximum line *height* [compare Fig. 2(a) and Fig. 3].

It is instructive to study the *temporal* evolution of the height and temperature in the region near the position of the laser beam (Fig. 4). Note, that the time dependence $h(t)$ differs from the spatial profile of the height in the center of the line [Fig. 2(a)], because growth continues also *behind* the laser beam. Figure 4 shows sharp jumps in the temperature and a much smoother behavior of the height. A similar be-

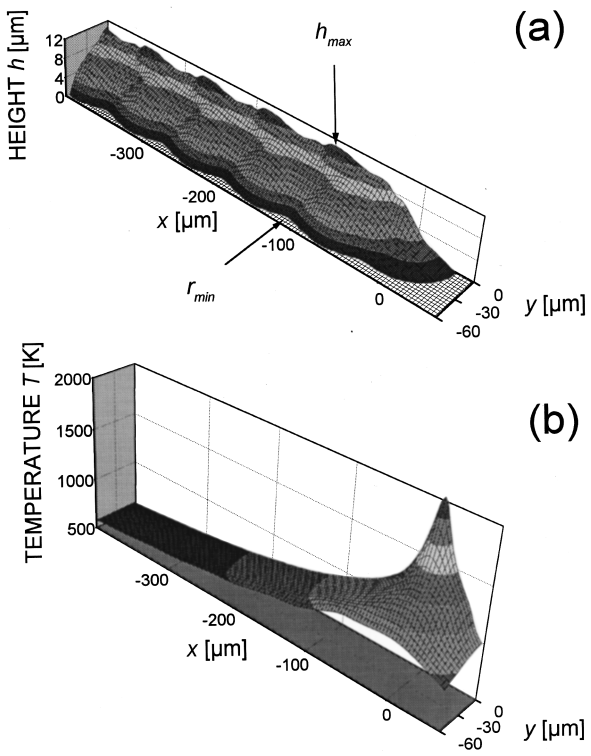

FIG. 2. Simulated height profile (a) and temperature distribution (b) of a W line for a temperature-dependent absorptivity (3.2) with $A_0=0.4$, $A_1=0.4$, $T_{\mathrm{Ab}}=1500$ K, and $\delta T_{\mathrm{Ab}}=10$ K. Other parameters as in Fig. 1.

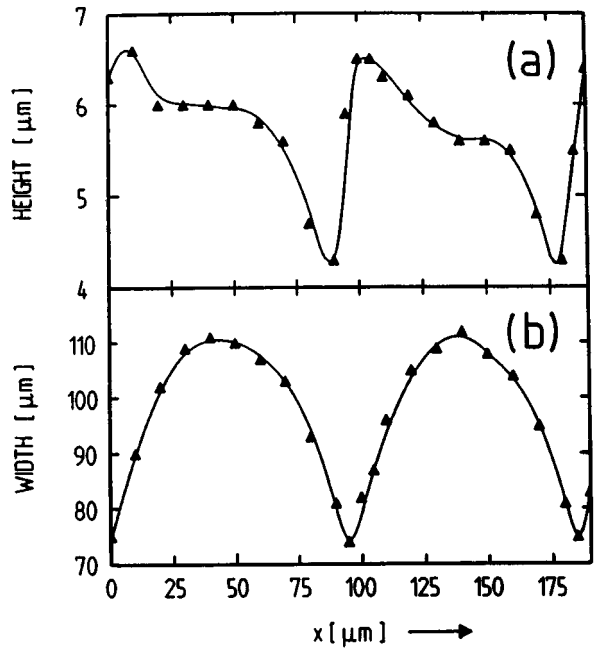

FIG. 3. Measured height (a) and width (b) of a W line deposited from 1.1 mbar/50 mbar/15 μbar $WCl_6+H_2+O_2$ (Ref. 6). The values of w_0, P, and v_s are the same as in Fig. 1.

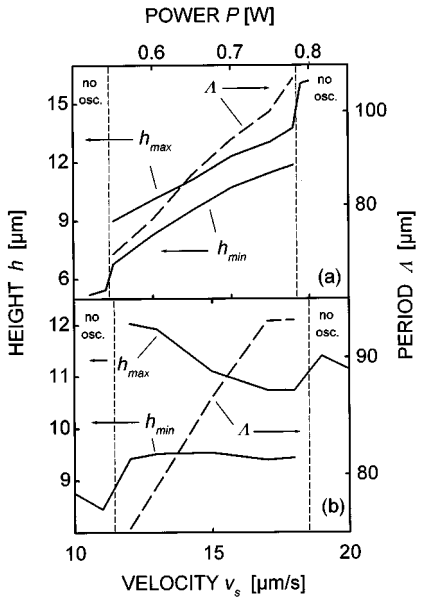

FIG. 5. Calculated dependence of the spatial period Λ (dashed line), and maximal and minimal height (solid lines) of a stripe. (a) Dependence on laser power. $v_s=15\ \mu$m/s. (b) Dependence on scanning velocity for $P=0.65$ W. Other parameters as in Fig. 2.

havior was found with the simplified model, which uses *two ordinary* differential equations.[22] This implies that the main features of the deposition dynamics can be understood in terms of only two ''order parameters'' h and T, the latter being the fast variable.

The dependence of the spatial period of oscillations, Λ, on laser power P is shown in Fig. 5(a) together with the maximum and minimum height of the deposited line. The same dependences on scanning velocity are shown in Fig. 5(b). Oscillations exist only in a finite interval of P and v_s.[6,22] Both h and Λ increase almost linearly with P. Λ increases also with v_s. In the region of uniform growth (Fig. 1), h decreases with v_s. All of these dependences agree within 15%–20% with those observed experimentally.[6] An even better agreement would require the exact knowledge of $A(T)$ and heat conductivity $K_D(T)$, which may differ from that of bulk tungsten. Additionally, experimental parameters, such as the laser power and spot size are also measured with an accuracy of only about 5%–10%.

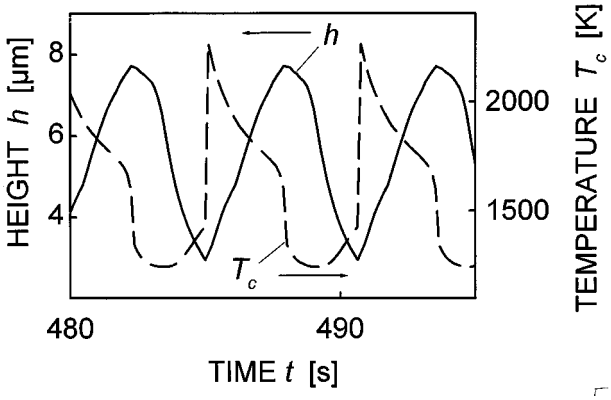

FIG. 4. Time-dependent behavior of the height (solid line) and temperature (dashed line) in the center of the laser beam for the parameters used in Fig. 2.

Another interesting point is the behavior of h near the limits of existence of oscillations. h jumps to lower/higher values at laser powers and scanning velocities below/above the region of oscillations. Consider, for example, the *decrease* in laser power. As long as oscillations exist, the system periodically reaches the ''high-temperature state'' with a high absorptivity near the center of the laser beam. This occurs when the height passes its *minimum* (see Fig. 4). When the oscillations disappear, the deposit near the laser spot is *always* in the low-temperature (and absorptivity) state. Thus, *below* the oscillation threshold, the deposition rate and the height of the stripe will be *smaller* than that corresponding to the minimal height within the oscillating line. Similar considerations apply to the upper boundary of existence of oscillations with respect to P or v_s.

IV. OSCILLATION OF LINES WITH HIGH ASPECT RATIO

Another interesting, and more general type of oscillations arises when the aspect ratio $\Gamma=h/r$, $2r$ being the linewidth, becomes of the order of unity (thick stripes). An example is the deposition of Si from SiH_4 onto quartz substrates.[7] Here, oscillations are observed with increasing Γ (mainly due to an increase in h), irrespective of whether this is caused by an *increase* in P or *decrease* in v_s. An example for the former case is shown in Fig. 6. When decreasing v_s, or increasing P even further, a series of almost equidistant fibers popping up from the substrate is formed. A similar behavior was observed during deposition of C from CH_4, C_2H_2, and C_2H_4 onto different substrates.[8] Subsequently, we

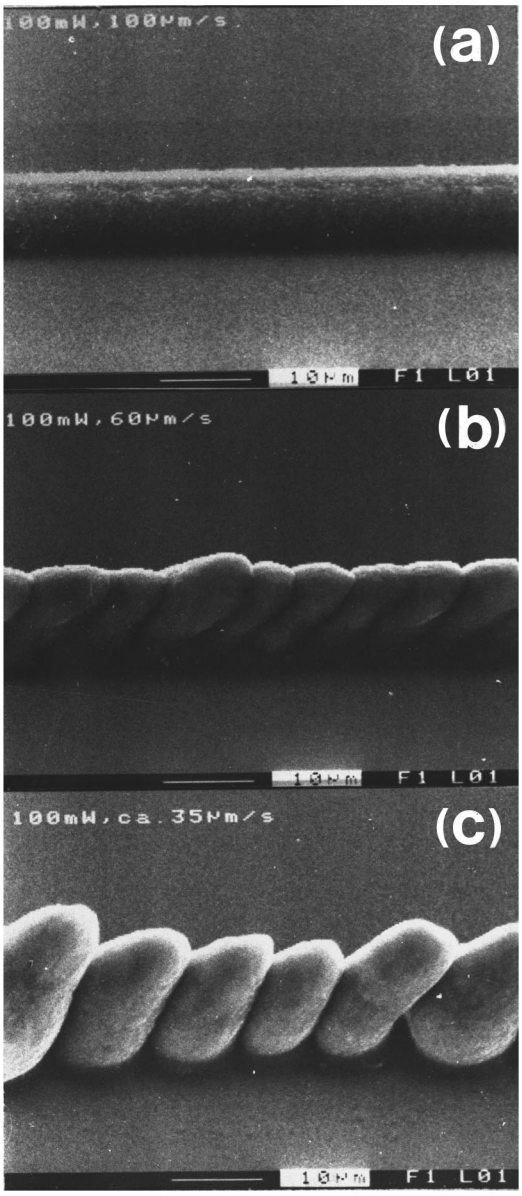

FIG. 6. Transition from continuous deposition of Si at high v_s to an oscillating regime at smaller v_s (500 mbar SiH_4, a-SiO_2 substrate, $w_0 = 2.5\ \mu$m, $P = 0.1$ W (Refs. 7 and 8)). (a) $v_s = 100\ \mu$m/s. (b) $v_s = 60\ \mu$m/s. (c) $v_s = 35\ \mu$m/s.

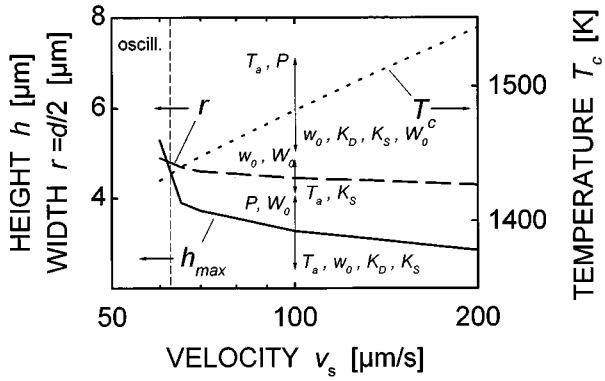

FIG. 7. Calculated dependence of (maximal) height (solid line), width (dashed line) and the maximal temperature (dotted line) for Si lines deposited from SiH_4. The values of w_0 and P are the same as in Fig. 6. Surface absorption with $A(T) = 0.635 - 5 \times 10^{-5} \times T$. The other parameters are listed in Table I. Arrows indicate the influence of different parameters on the calculated dependences as described in the text. Near $v_s = 60\ \mu$m/s, a transition to explosive growth occurs.

apply our algorithm to the deposition of Si from SiH_4. The parameters employed are included in Table I and in the figure captions. Unlike the $WCl_6 + H_2$ system, SiH_4 does not possess an abrupt temperature threshold for deposition, and the reaction rate in Eq. (2.1) can be approximated by a simple Arrhenius function:[1]

$$W(T) = W_0 \exp(-T_a/T). \tag{4.1}$$

Let us study the changes in the calculated shape of stripes with decreasing v_s. With high scanning velocities, the profile of stripes and temperature distributions is qualitatively similar to that shown in Figs. 1 and 2(b), respectively. With decreasing v_s, both h and r increase, while the temperature near the center of the laser beam, T_c, decreases due to heat conduction along the stripe (Fig. 7). A semiquantitative analysis of this behavior in a 1D approximation was given in Ref. 16. The arrows in Fig. 7 illustrate the influence of different parameters onto calculated dependences. The direction of the arrows shows the shift in the dependence with an *increase* of the corresponding parameter, when all other parameters are kept constant. The parameters are listed in an order that reflects the decrease in the magnitude of the changes. For example, T_c increases with T_a and P, but decreases with heat conductivities K_D and K_S. An increase in the laser-beam spot size w_0 and the pressure of the precursor (preexponential factor W_0) also decreases T_c. Within a certain range, r is almost independent of P and K_D. Both h and r decrease with increasing T_a because the growth rate increases with temperature more sharply and all changes take place within a smaller spatial region.

When v_s becomes small enough, *damped* oscillations in the height of the stripes appear. If v_s is even further decreased, *persistent* oscillations are observed. In Fig. 7, $h_{\max}$ corresponds to the *maxima* of these oscillations. With very low velocities, the oscillations become unstable, and the ''humps'' are transformed into fibers, which grow towards the laser beam [Fig. 8(a)]. The corresponding temperature distribution is shown in Fig. 8(b). A similar sequence of deposition regimes is obtained if the laser power is gradually increased. Subsequently, we analyze the main reasons for this behavior.

One reason is a nontrivial dependence of T_c on h. Let us demonstrate this by studying the changes in T_c at the top of a spot-shaped deposit, which shall be a much better heat conductor than the substrate. The radius of the deposit shall be fixed. The light shall be absorbed at the upper surface, which is a good approximation for metals and also for semiconductors at elevated temperatures. Initially, T_c will decrease with h due to a better *lateral* heat conduction within the *thicker* spot. When $\Gamma = h/r$ becomes comparable to unity, T_c starts to increase due to the increasing temperature difference within the deposit in the direction *normal* to the substrate surface. This results in a positive feedback, which

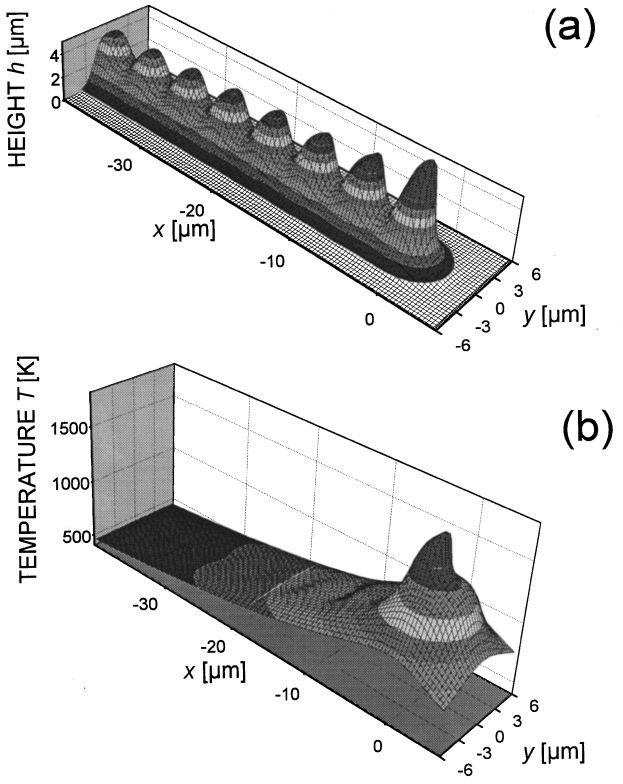

FIG. 8. Simulation of a line–fiber transition for Si deposited from SiH_4, $v_s = 60\ \mu$m/s. (a) Height profile. (b) Temperature distribution on the upper surface of the deposit.

leads to explosive growth.[17] A similar behavior holds for stripes, as discussed for the 1D approximation.[16] This mechanism is dominating for Si deposition.

Another reason is related to the front edge of the thick stripes. Because growth takes place normal to the surface, the front edge of the stripes is even narrower than the width of the reaction zone. At very small v_s, it flips over.[18] Further complications arise from the decrease in absorptivity via the oblique incidence of the laser beam on the *steep* front edge, which may terminate the deposition process. This mechanism may also contribute to the oscillatory behavior.

A third reason is related to the fact that both the width of the deposited line and the temperature distribution exceed that of the laser beam. As a result, the maximal temperature (which is achieved *on the front slope* of the deposited line) is mainly determined by the cross section of the line *behind* the laser beam, i.e., by the parts of the stripe deposited *previously*. This may lead to an *inertial* feedback.[24]

These three factors influence the deposition dynamics in different ways. A numerical analysis shows that the latter mechanism (delayed feedback) alone, does not produce oscillations, in contrast to the former two. The region of the parameters where oscillations occur may change significantly if any of the mechanisms are ''switched off.'' In the general case, the first two mechanisms *cannot* be separated because both of them become important with $\Gamma \sim 1$.

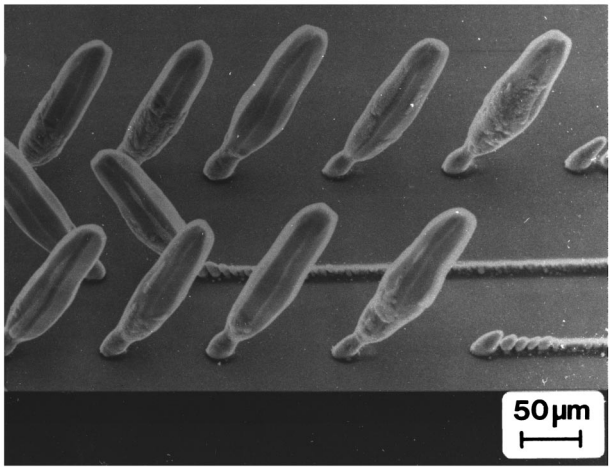

FIG. 9. Line–fiber transition and hysteresis with respect to scanning velocity for the deposition of Si from 500 mbar SiH_4 ($w_0 = 1.5\ \mu$m, $P = 0.136$ W). For the upper and lower scans, v_s was *increased* from left to right. For the scan in the middle, v_s was *decreased* from right to left.

V. HYSTERESIS IN THE TRANSITION FROM LINE- TO FIBER-TYPE GROWTH

In contrast to the *oscillating* regime of line-type growth, the regime of fiber-type growth (Fig. 8) can be explained only by the increase in T_c with h. The fiber grows towards the laser beam in a quasisteady regime.[19] The focused laser beam diverges, and its size becomes comparable to the diameter of the fiber. As a result, the absorbed laser power decreases, growth terminates, and the laser beam again reaches the substrate. A new fiber grows in the region where no deposited line is present. Then the process repeats, and a series of separated fibers is formed.

The transition between the two regimes (Fig. 9) shows a pronounced hysteresis with laser power and scanning velocity.[7,8] The physical reason for this can be illustrated as follows: Consider an *increase* in laser power (line–fiber transition). The formation of a fiber occurs around a certain temperature. If the laser power is *decreased* (fiber–line transition), this temperature is reached at a *lower* value of P, just because the heat loss *into the deposited stripe* is absent. A similar picture is observed if v_s is decreased for the line–fiber transition and then increased to restore continuous deposition.

The hysteresis has also been simulated. However, the difference in temperature distributions for lines and spots was found to be so large that the calculated v_s *for fiber–line transitions* were much higher than the experimental values. As a result, the width of the hysteresis was significantly overestimated. The reason for this inconsistency is that with the laser powers employed, the temperature that is induced at the substrate in the *initial* stage of growth is very high. With such temperatures, the deposition reaction becomes transport limited and the growth rate can be approximated by[1]

$$W(T) = \frac{W_0 \exp(-T_a/T)}{1 + a \exp(-T_a/T)}, \tag{5.1}$$

with

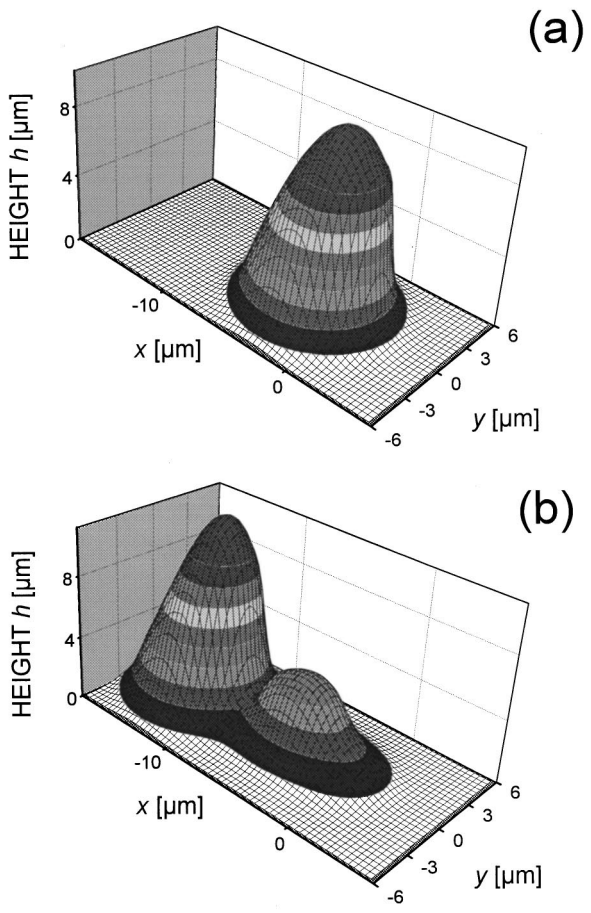

FIG. 10. (a) Formation of a *fiber* from a spot with $v_s = 65\ \mu$m/s, (b) Initial stage of *line* formation from a spot with $v_s = 75\ \mu$m/s. Other parameters as in Fig. 7.

$$a = \frac{\rho_d}{\rho_g}\frac{W_0 R}{D}. \tag{5.2}$$

Here, ρ_d and ρ_g are the densities *of the deposited species* in the solid and the gas phase, respectively. D is the gas-phase diffusion coefficient, and R the radius of the reaction zone. The temperature dependence of a is weak in comparison to the exponential function and it was ignored. Because of the uncertainties associated with Eq. (5.2), a was considered as a fitting parameter. With the experimental setup employed, transport limitation starts around $T \approx 1500$ K.[25] This can be described by Eq. (5.1) with $a = 8 \times 10^5$, which was used in the calculations.

Because the characteristic temperatures for the deposition of thick lines are rather low (Fig. 7), transport limitations play an important role only in the initial stage of growth. The *initial* radius of the growing spot is determined by the area where the temperature induced on the substrate exceeds the temperature at which diffusion limitations start. As a result, this radius is much wider than it would have been in the case of a kinetically controlled process. An increase in the initial radius of the spot leads to a narrowing of the hysteresis with respect to P and v_s because it facilitates heat conduction into the substrate, thus, lowering the temperature of the spot.

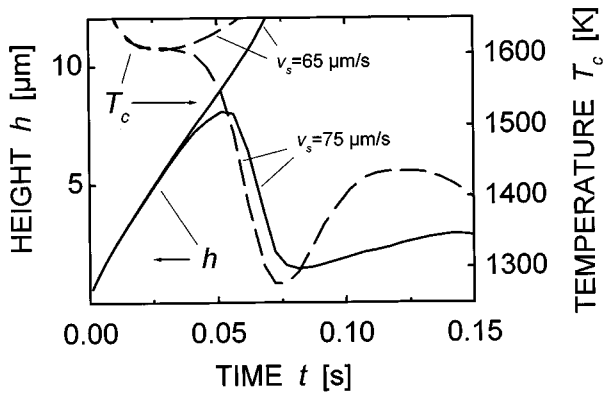

FIG. 11. The behavior of the height (solid lines) and temperature (dashed lines) in the center of the laser beam as functions of time. Initial stages of deposition with $v_s = 65\ \mu$m/s and $v_s = 75\ \mu$m/s (see Fig. 10). In the latter case, transition to line deposition with damped oscillations can be seen.

If the scanning velocity is gradually *lowered* to $v_s = 65\ \mu$m/s, simulations result in oscillating lines. When no line is initially present, the formation of a fiber is observed for *the same* set of parameters [Fig. 10(a)]. When the scanning velocity is increased up to 75 μm/s, fiber formation ceases and, after a transition regime [Fig. 10(b)], a continuous line is formed. The transient profiles are quite similar to those observed experimentally (Fig. 9, lower scan).

The temporal dependences of h and T_c (near the position of the laser beam) are illustrated in Fig. 11 for $v_s = 65\ \mu$m/s and $v_s = 75\ \mu$m/s. If the scanning velocity is high enough, the transition to explosive-type growth does not occur.

Figure 12 shows the calculated boundary, which separates regions of continuous line-type deposition and fiber-type growth as a function of scanning velocity and laser power. This behavior agrees quite well with that observed experimentally.[8,16]

An additional note seems to be appropriate. The accuracy of the numerical simulations is determined by the accuracy to which the thermophysical parameters and the real dependence of the absorptivity on temperature are known. For the W system, this accuracy is high enough to achieve quantitative agreement with the experimental results. In the case of Si, however, only a semiquantitative agreement was achieved. This is mainly due to the strong temperature dependence of the heat conductivity of silicon and the high activation energy of the SiH_4 decomposition reaction. Thus, even small uncertainties in parameters, or small systematic errors in the algorithm for θ_{Si} may produce significant deviations from the experimental data, especially with respect to the scanning velocity, which is almost exponentially related to the calculated temperature.

VI. CONCLUSIONS

We have presented numerical simulations of pyrolytic laser direct writing based on a fast algorithm for temperature calculations.[17] This approach allows one to model oscilla-

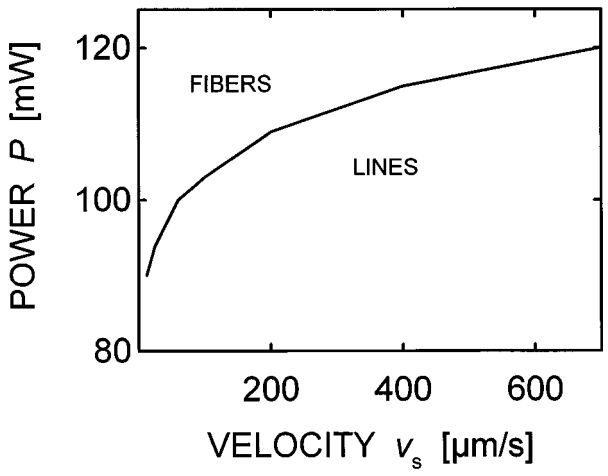

FIG. 12. Calculated boundary between regimes of continuous deposition of lines and the formation of fibers.

tions observed in laser CVD. These oscillations are caused by the coupling of the shape of the deposit and the temperature distribution induced by the laser beam.

In the case of W deposition from an admixture of $WCl_6+H_2+O_2$ onto a-SiO_2 substrates, the oscillations in height and width of deposited lines are due to a sharp increase in the absorptivity of the deposit within a narrow temperature interval.[16,22] Simulations reproduce the dependence of the period of oscillations on laser power and scanning velocity, and they also explain the shape of deposited lines.

With the deposition of Si from SiH_4 onto a-SiO_2 substrates, the oscillations are caused by temperature differences between the upper surface of the deposit and the substrate. With decreasing scanning velocity or increasing laser power, initially continuous lines show oscillations, mainly in height, and a transition to explosive-type growth results in fiber formation.

The hysteresis in this transition with increasing/decreasing laser power/scanning velocity can be explained as well.

The proposed algorithm allows a quantitative self-consistent analysis of the pyrolytic deposition of microstructures. It can also be used for the modeling of pyrolytic etching and e-beam microprocessing when feedbacks between temperature distributions and changes in processing geometries are important.

ACKNOWLEDGMENTS

The authors wish to thank Dr. R. Kullmer for some of the experimental data that were analyzed in this article, Professor B. Luk'yanchuk for valuable discussions, and the ''Fonds zur Förderung der Wissenschaftlichen Forschung in Österreich'' Project No. P 10406-PHY for financial support.

[1] D. Bäuerle, *Laser Processing and Chemistry* (Springer, Berlin, 1996), p. 497.
[2] *Laser Microfabrication—Thin Film Processes and Lithography*, edited by D. J. Ehrlich and J. Y. Tsao (Academic, New York, 1989).
[3] S. Preuβ and H. Stafast, Appl. Phys. A **54**, 152 (1992).
[4] F. Foulon and M. Stuke, Appl. Phys. A **56**, 283 (1993).
[5] J. Messelhäuser, E. B. Flint, and H. Suhr, Appl. Phys. A **55**, 196 (1992).
[6] P. B. Kargl, R. Kullmer, and D. Bäuerle, Appl. Phys. A **57**, 175 (1993).
[7] P. B. Kargl, R. Kullmer, and D. Bäuerle, Appl. Phys. A **57**, 577 (1993).
[8] P. B. Kargl, N. Arnold, and D. Bäuerle, Appl. Surf. Sci. **108**, 257 (1997).
[9] T. H. Baum and P. B. Comita, Thin Solid Films **218**, 80 (1992).
[10] M. L. Burgener and R. E. Reedy, J. Appl. Phys. **53**, 4357 (1982).
[11] M. Lax, J. Appl. Phys. **50**, 3919 (1977).
[12] K. Piglmayer, J. Doppelbauer, and D. Bäuerle, in *Laser Controlled Chemical Processing of Surfaces*, edited by A. W. Johnson, D. J. Ehrlich, and H. R. Schlossberg (North-Holland, New York, 1984), p. 47.
[13] C. Garrido, B. Leon, and M. Perez-Amor, J. Appl. Phys. **69**, 1133 (1991).
[14] J. Han and K. F. Jensen J. Appl. Phys. **75**, 2240 (1994).
[15] N. Arnold, R. Kullmer, and D. Bäuerle, Microelectron. Eng. **20**, 31 (1993).
[16] N. Arnold, P. B. Kargl, and D. Bäuerle, Appl. Surf. Sci. **86**, 457 (1994).
[17] N. Arnold J. Appl. Phys. **80**, 1291 (1996).
[18] N. Kirichenko, Y. Khavin, and N. Arnold, Appl. Surf. Sci. **93**, 359 (1996).
[19] N. Arnold, E. Thor, N. Kirichenko, and D. Bäuerle, Appl. Phys. A **62**, 503 (1996).
[20] W. H. Press, S. A. Teukolsky, W. T. Vetterling, and B. P. Flannery, *Numerical Recipes in FORTRAN (also C or Pascal)* (Cambridge University Press, New York, 1992).
[21] N. Arnold and D. Bäuerle, Microelectron. Eng. **20**, 43 (1993).
[22] N. Arnold, P. B. Kargl, R. Kullmer, and D. Bäuerle, Appl. Phys. A **61**, 347 (1995).
[23] R. Kullmer, P. B. Kargl, and D. Bäuerle, Thin Solid Films **218**, 122 (1992).
[24] Y. C. Du, U. Kempfer, K. Piglmayer, D. Bäuerle, and U. M. Titulaer Appl. Phys. A **39**, 167 (1986).
[25] J. Doppelbauer and D. Bäuerle, in *Interfaces Under Laser Irradiation*, NATO ASI Series E, edited by L. D. Laude, D. Bäuerle, and M. Wautelet (Martinus Nijhoff, Dordrecht, 1987), Vol. 134, p. 277.